

The puzzling merging cluster Abell 1914: new insights from the kinematics of member galaxies

R. Barrena^{1,2*}, M. Girardi^{3,4} and W. Boschin⁵

¹*Instituto de Astrofísica de Canarias, C/Vía Láctea s/n, E-38205 La Laguna (Tenerife), Spain*

²*Departamento de Astrofísica, Univ. de La Laguna, Av. del Astrofísico Francisco Sánchez s/n, E-38205 La Laguna (Tenerife), Spain*

³*Dipartimento di Fisica dell'Università degli Studi di Trieste - Sezione di Astronomia, via Tiepolo 11, I-34143 Trieste, Italy*

⁴*INAF - Osservatorio Astronomico di Trieste, via Tiepolo 11, I-34143 Trieste, Italy*

⁵*Fundación G. Galilei - INAF (Telescopio Nazionale Galileo), Rambla J. A. Fernández Pérez 7, E-38712 Breña Baja (La Palma), Spain*

Accepted DATE. Received DATE; in original form DATE

ABSTRACT

We analyze the dynamical state of Abell 1914, a merging cluster hosting a radio halo, quite unusual for its structure. Our study considers spectroscopic data for 119 galaxies obtained with the Italian Telescopio Nazionale Galileo. We select 89 cluster members from spatial and velocity distributions. We also use photometry Canada-France-Hawaii Telescope archives. We compute the mean cluster redshift, $\langle z \rangle = 0.168$, and the velocity dispersion which shows a high value, $\sigma_V = 1210^{+125}_{-110}$ km s⁻¹. From the 2D analysis we find that Abell 1914 has a NE-SW elongated structure with two galaxy clumps, that mostly merge in the plane of the sky. Our best, but very uncertain estimate of the velocity dispersion of the main system is $\sigma_{V,\text{main}} \sim 1000$ km s⁻¹. We estimate a virial mass $M_{\text{sys}} = 1.4\text{--}2.6 \times 10^{15} h_{70}^{-1} M_{\odot}$ for the whole system. We study the merger through a simple two-body model and find that data are consistent with a bound, outgoing substructure observed just after the core crossing. By studying the 2D distribution of the red galaxies, photometrically selected, we show that Abell 1914 is contained in a rich large scale structure, with two close companion galaxy systems, known to be at $z \sim 0.17$. The system at SW supports the idea that the cluster is accreting groups from a filament aligned in the NE-SW direction, while that at NW suggests a second direction of the accretion (NW-SE). We conclude that Abell 1914 well fits among typical clusters with radio halos. We argue that the unusual radio emission is connected to the complex cluster accretion and suggest that Abell 1914 resembles the well-known nearby merging cluster Abell 754 for its particular observed phenomenology.

Key words: Galaxies: clusters: general. Galaxies: cluster: individual: Abell 1914.

1 INTRODUCTION

A fraction of galaxy clusters shows the presence of diffuse radio emission on Mpc scale. In general, we can distinguish between two morphologies: “radio halos” and “radio relics”. In the first case, the emission comes from central cluster regions, while “relics” take place in the peripheral zones (Giovannini et al. 2002; Ferrari et al. 2008; Venturi 2011; Feretti et al. 2012). The synchrotron origin of this radio emission reveals the presence of a large-scale magnetic field and relativistic particles spread out of the cluster. Nowadays, cluster mergers seem to be the most reasonable framework proposed to provide enough energy for accelerating electrons to relativistic velocities and for magnetic field amplification. In

this scenario, radio relics seem to be directly linked with merger shocks (Ensslin et al. 1998; Roettiger et al. 1999; Ensslin & Gopal-Krishna 2001; Hoeft et al. 2004). Instead, the turbulence following cluster mergers has been proposed as one of the most important effects to produce giant radio halos (Brunetti et al. 2001, 2009). However, the precise scenario for radio halo formation is still debated. In fact, there are two main theoretical approaches to the problem: re-acceleration vs. hadronic models (Brunetti et al. 2009 and refs. therein).

Usually, X-ray observations are used to study the dynamical state of clusters with diffuse radio emission. Indeed, all statistical analyses are derived from X-ray data (Schuecker et al. 2001; Buote 2002; Cassano et al. 2010; Rossetti et al. 2011) and properties of radio emission are derived in general from X-ray temperature and luminosity

* E-mail: rbarrena@iac.es

(see e.g. Giovannini et al. 2002, and references therein). In fact, predictions based on turbulent re-acceleration models well agree with the radio observations of halos (Cassano et al. 2006). In this sense, Govoni et al. (2001) also find a strong correlation between X-ray and radio emission when they compare point-to-point individual surface brightnesses. In addition, Basu (2012) reveal no evidence of bimodality in the radio-power – integrated SZ effect diagram while, at the contrary, Brunetti et al. (2007) find this bimodal feature in the radio-power – X-ray luminosity diagram. This fact reveals the need to manage other research ways in addition to X-ray techniques.

Optical information is an important way to investigate the dynamics of cluster mergers (Girardi & Biviano 2002). The spatial distribution and kinematics of galaxy members allow us to detect substructures and to analyze possible pre- and post-merging groups, and to distinguish between evolving mergers and remnants. Moreover, optical data are complementary to X-ray information because the ICM and galaxies react on different timescales during a collision. This is clearly shown in numerical simulations by Roettiger et al. (1997). Thus, for example, the importance of combining X-ray and optical data to study merging scenarios is shown by MUSIC (MULTI-Wavelength Sample of Interacting Clusters) project (Maurogordato et al. 2011).

In this context, we are now progressing on the DARC (Dynamical Analysis of Radio Clusters, see Girardi et al. 2010¹) project, which uses spectroscopic and photometric information of galaxy members to analyze the internal dynamics of clusters with diffuse radio emission.

We have carried out an intensive observational program focused on the cluster of galaxies Abell 1914 (hereafter A1914). A1914 is a rich cluster, X-ray luminous, hosting a hot ICM. It shows an Abell richness class $R = 2$ (Abell et al. 1989), $L_X(0.1\text{--}2.4\text{ keV}) = 17.93 \times 10^{44} h_{70}^{-2} \text{ erg s}^{-1}$ (Ebeling et al. 1996) and $kT_X \sim 9\text{ keV}$ (Baldi et al. 2007; Maughan et al. 2008). Following the Bautz-Morgan classification, A1914 is a type II structure (Abell et al. 1989), while it is a “L-type” (“linear”) cluster in the Rood-Sastry morphological scheme (Struble & Rood 1987).

Dahle et al. (2002) study the mass and light distributions using weak-lensing techniques. They recover the elongated shape of this cluster in the NE-SW direction and find that the light distribution well follows the mass profile. The two brightest cluster galaxies trace the two highest peaks in the mass distribution, although in the reverse order, that is, the highest peak is close to the second brightest galaxy (Okabe & Umetsu 2008). On the other hand, Jones et al. (2005) analyze the galaxy distribution in the POSS digital. They find signs of dynamical activity with two distinct groups of galaxies with no single dominant galaxy.

Buote & Tsai (1996) develop the first analysis of the X-ray morphology of this cluster using ROSAT data. They find that A1914 is a relaxed structure, but Jones et al. (2005) show some evidence against this thesis, suggesting that this cluster is not so relaxed. They find no evidence for a cool core, an unusual high X-ray temperature, and notice that ROSAT data are very poorly fitted using a β model. Then,

using Chandra X-ray data, Govoni et al. (2004) show clear evidence of merger. In fact, they find a clear elongation of the X-ray surface brightness (along WNW-ESE, see Fig. 5d of Govoni et al. 2004). In the last years, using Chandra data, A1914 has been classified as a non relaxed cluster (Baldi et al. 2007; Maughan et al. 2008).

Concerning the radio emission, Komissarov & Gubanov (1994) first report evidence for a diffuse and extended radio source (see also Giovannini et al. 1999; Kempner & Sarazin 2001). Moreover, Bacchi et al. (2003), using VLA data, show the presence of a unpolarized halo. The halo covers a $7.4' \times 5.3'$ area with a power $P_{1.4\text{ GHz}} = 8.72 \times 10^{24} h_{70}^{-2} \text{ W Hz}^{-1}$. Govoni et al. (2004) point out that the diffuse radio emission is quite puzzling with a bright component elongated in the NW-SE direction and a more typical low-brightness halo in the cluster center (see Fig. 5d of Govoni et al. 2004). The bright radio region does not follow either the elongation of the X-ray surface brightness. This fact is quite unusual, because in the majority of clusters the elongated diffuse radio halo follows the direction of the merger (e.g., the “Bullet” Cluster 1E0657-56, Markevitch et al. 2002; but see Abell 523, Giovannini et al. 2011).

Despite several studies based on X-ray data, published redshift data are not enough to perform the detailed dynamical study of A1914. The work we present here is based on new spectroscopic data obtained with the Telescopio Nazionale Galileo (TNG). We also use photometric data from the Canada-France-Hawaii Telescope (CFHT) archive.

This paper is organized as follows. We present optical data, including redshifts and photometry information, in Sect. 2. We expose our results on the cluster structure in Sect. 3. The discussion on the dynamical state of A1914 and conclusions are presented in Sect. 4 and 5, respectively.

Unless otherwise stated, we present errors at the 68% confidence level (hereafter c.l.). Along this paper, we work using $H_0 = 70 \text{ km s}^{-1} \text{ Mpc}^{-1}$ and $h_{70} = H_0/(70 \text{ km s}^{-1} \text{ Mpc}^{-1})$ and a flat cosmology with $\Omega_0 = 0.3$ and $\Omega_\Lambda = 0.7$. Within this cosmology, $1'$ corresponds to $\sim 172 h_{70}^{-1} \text{ kpc}$ at the cluster redshift.

2 THE DATA SAMPLE

2.1 Spectroscopic data

We performed observations of A1914 using DOLORES multi-object spectrograph at the TNG telescope in March 2010. We used the LR-B grism, which provides a dispersion of 187 \AA/mm . DOLORES works with a 2048×2048 pixels E2V CCD. The pixel size is $13.5 \mu\text{m}$. We retrieved a total of 4 MOS masks containing 146 slits. We exposed 3600 s for each mask.

Spectra were reduced using standard IRAF² tasks. Radial velocities were computed by using the cross-correlation technique (Tonry & Davis 1979) with the IRAF/XCSAO task, as we have proceeded with other clusters already analyzed in the DARC project (for a detailed description, see

¹ see also <http://adlbitum.oat.ts.astro.it/girardi/darc>, the web site of the DARC project.

² IRAF is distributed by the National Optical Astronomy Observatories, which are operated by the Association of Universities for Research in Astronomy, Inc., under cooperative agreement with the National Science Foundation.

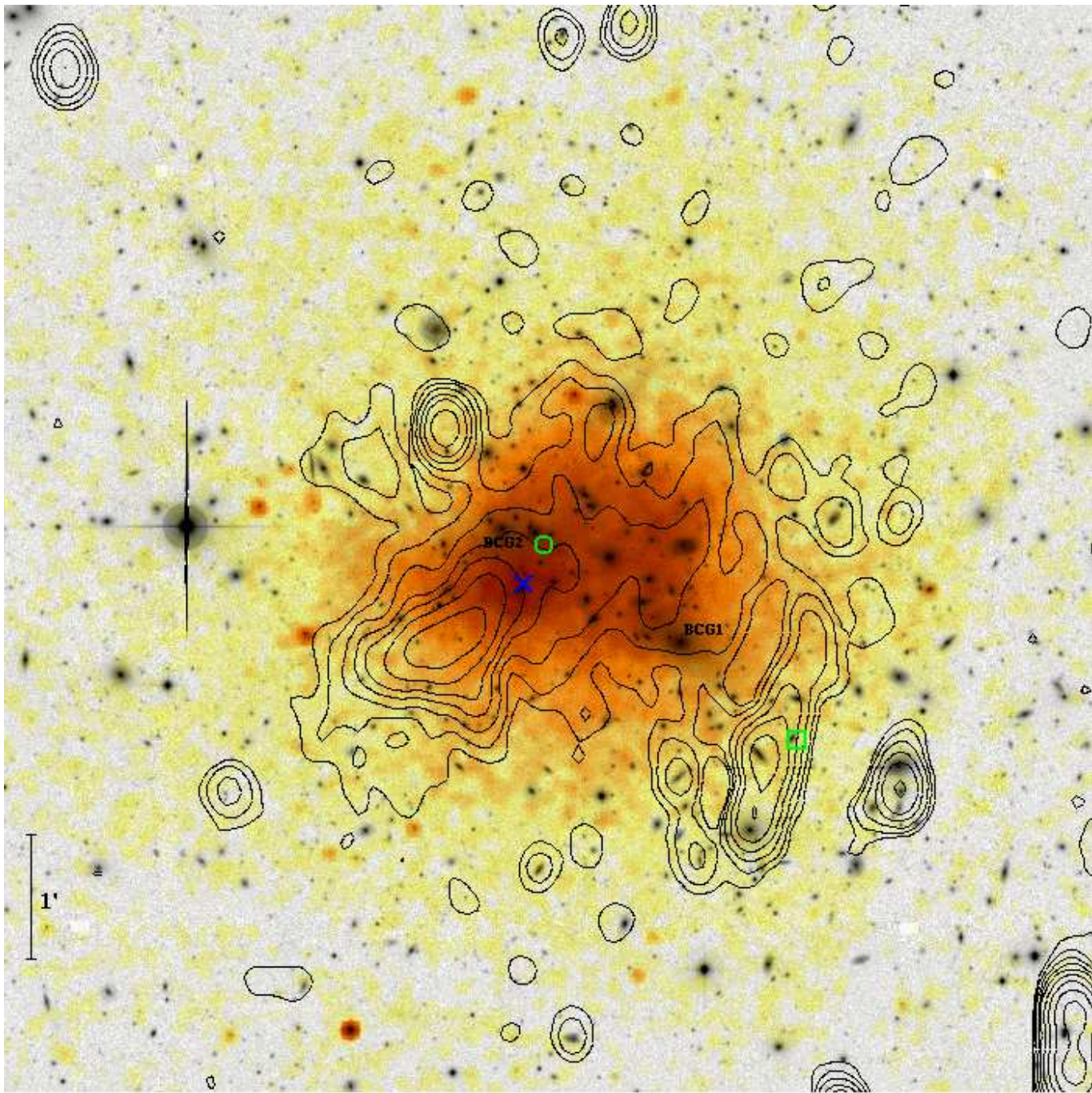


Figure 1. Multiwavelength image of the central region of A1914. The gray-scale image in background corresponds to the optical r^{Mega} -band (CFHT archive). Superimposed, with orange and yellow colors, we also show the smoothed X-ray image in the 0.3-7 keV energy range (Chandra archive). Contour levels represent the VLA radio image at 1.4 GHz (courtesy of F. Govoni; see Bacchi et al. 2003). Green circle and square mark the centers of the density peaks detected in our analysis of the galaxy distribution (see Sect. 3.6). Blue "X" marks the centroid of the X-ray surface brightness (Govoni et al. 2004). Labels indicate the positions of the two brightest cluster galaxies (BCG1 and BCG2; see Sect. 2.2 and Table 1). North is up and East is left.

e.g. Boschin et al. 2012). In six cases (IDs. 78, 79, 83, 99, 100, 107 and 112; see Table 1), we considered the IRAF/EMSAO redshift (based on the wavelength of emission lines in the spectra) to get a realistic estimation. So, our catalog lists 113 galaxy redshifts in the field of A1914. We also considered six redshifts more from the SDSS archive (IDs. from 114 to 119; see Table 1).

The true intrinsic errors are larger than those formal errors given by the cross-correlation (e.g., Malumuth et al. 1992; Ellingson & Yee 1994; Quintana et al. 2000; Bardelli et al. 1994). To correct this effect, some galaxies were observed in more than one mask. This allows us to estimate the intrinsic errors in data of the same quality acquired with the same instrumentation. Our spectroscopic survey

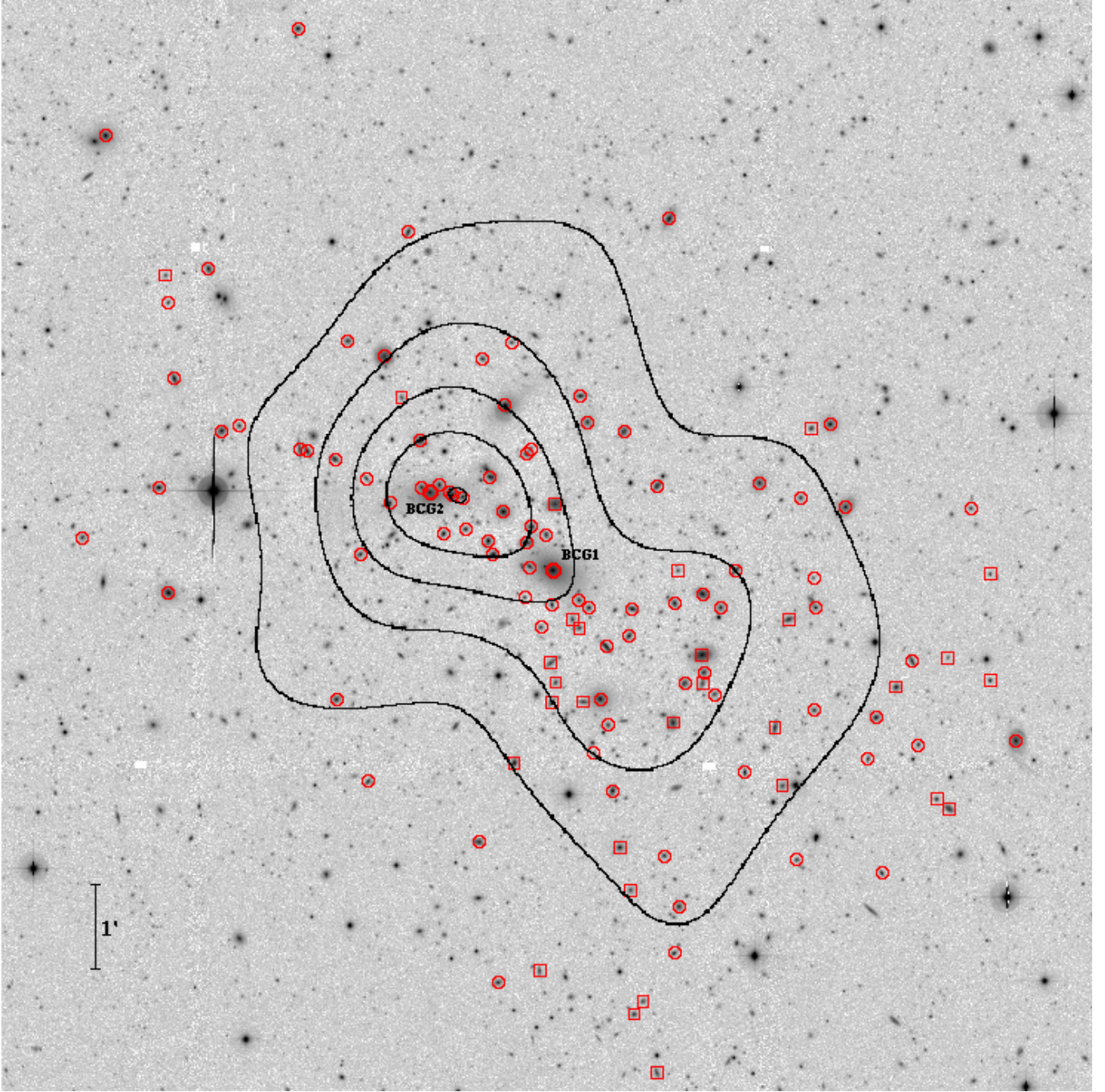


Figure 2. r^{Mega} -band image of Abell 1914 (CFHT archive). Circles and squares correspond to galaxy members and nonmembers, respectively (see Table 1). Labels and enhanced circles mark the positions of the two brightest cluster galaxies (BCG1 and BCG2; see Sect. 2.2 and Table 1). Black contours are the isodensity contours of the distribution of likely member galaxies (see Sect. 3.6 and Fig. 9-top panel). North is up and East is left.

provides duplicate estimations for 18 galaxies. So, following the method detailed in Barrena et al. (2009) for these 18 galaxies and using the weighted mean of the two measurement, we concluded that true intrinsic errors are larger than formal cross-correlation ones by a factor of two. For the redshifts estimated with the EMSAO task we considered the largest value between 100 km s^{-1} and the formal error.

We also considered nine galaxies having redshift in the SDSS and lying in the same field spanned by our spectro-

scopic data. Three of these SDSS targets were also observed with the TNG/DOLORES. We find no systematic deviations between the SDSS and our redshifts. We add the remaining six galaxies to our TNG catalog. Finally, we obtain a spectroscopic catalog of 119 galaxies, with a median value of the cz errors of 74 km s^{-1} .

2.2 Photometry and galaxy catalog

We also use public photometric data obtained with Megaprime/Megacam at the CFHT. In particular, we consider g^{Mega} and r^{Mega} band³ images retrieved from the CADC Megapipeline archive (Gwyn 2009). These images cover an area of $1.05 \times 1.16 \text{ deg}^2$ with a deepness of $g^{\text{Mega}} = 27.2$ and $r^{\text{Mega}} = 26.8$ limiting magnitudes (at the 5σ detection level). Megaprime photometry is 90% complete down to $g^{\text{Mega}} = 24.8$ and $r^{\text{Mega}} = 24.6$. We corrected g^{Mega} and r^{Mega} CFHT magnitudes for galactic extinction assuming extinction values obtained from SDSS (DR7) in the central cluster region.

Table 1 lists our velocity catalog and photometry (see also Fig. 2). We present an identification (ID) number in Col. 1 (galaxy members are listed in italic format); right ascension and declination (J2000) in Col. 2; CFHT r^{Mega} magnitudes in Col. 3; and heliocentric radial velocities $v = cz_{\odot}$ and errors Δv in Col. 4 and Col. 5, respectively.

Our spectroscopic sample is 80% (50%) complete down to $r' = 18.3$ ($=19.7$), within an elongated region of 60 arcmin^2 (corresponding to an area of $1.1 \times 1.6 \text{ Mpc}$ at the redshift of the cluster) around the cluster center.

The brightest cluster galaxy is ID. 29 ($r^{\text{Mega}} = 15.87$, hereafter BCG1). It lies at the south-west and is non-dominant (in luminosity) in the cluster. In fact, there is a second brightest cluster galaxy at the north-east (ID. 20, $r^{\text{Mega}} = 16.39$, hereafter BCG2). The two galaxies are separated by $\sim 1.7'$, i.e. $\sim 0.3 h_{70}^{-1} \text{ Mpc}$ at the cluster distance.

3 ANALYSIS OF THE OPTICAL DATA

3.1 Cluster member selection

In order to select cluster members we followed a procedure with two steps. First, we run the 1D adaptive-kernel method (hereafter 1D-DEDICA, Pisani 1993 and 1996; see also Girardi et al. 1996; Fadda et al. 1996). We detected significant peaks (at $>99\%$ c.l.) in the velocity distribution. This procedure found A1914 as a peak at $z \sim 0.1675$, containing 100 (provisional) cluster candidates (in the range $45\,921 \leq v \leq 58\,839 \text{ km s}^{-1}$, see Fig. 3). We also found 18 and 1 background and foreground galaxies, respectively.

Then, in a second step, we only consider the 100 likely cluster candidates to run the “shifting gapper” method proposed by Fadda et al. (1996; see also, e.g., Girardi et al. 2011), which takes into account a combination of velocity and position of the galaxies. This method needs the definition of a cluster center, but the optical center of A1914 is not obvious due to the absence of a clear dominant galaxy and to the offset of the X-ray center (e.g., Maughan et al. 2008). So, we decided to assume as cluster center the position of BCG1 (see Table 1). The application of the “shifting gapper” rejected another eleven galaxies leading to a final sample of 89 cluster members (Fig. 4 – top panel).

In order to check the robustness in the galaxy member selection and estimate how the choice of cluster center

[lht]

Table 1. Radial Velocities of 119 galaxies in the field of Abell 1914. † and ‡ denote the BCG1 and BCG2, respectively.

ID	α, δ (J2000)	r^{Mega}	v (km s ⁻¹)	Δv
<i>01</i>	14 26 11.65, +37 55 16.6	18.44	50860	50
<i>02</i>	14 26 19.43, +37 52 24.7	20.43	55260	134
<i>03</i>	14 26 19.27, +37 52 05.7	20.20	50340	102
<i>04</i>	14 26 16.90, +37 52 29.1	18.53	50375	32
<i>05</i>	14 26 18.91, +37 51 12.6	18.02	52280	30
<i>06</i>	14 26 24.30, +37 49 21.9	19.58	49505	64
<i>07</i>	14 26 19.83, +37 49 56.7	17.97	50539	40
<i>08</i>	14 26 16.13, +37 50 36.3	18.28	49964	44
<i>09</i>	14 26 15.09, +37 50 39.9	19.76	49591	82
<i>10</i>	14 26 05.16, +37 52 54.9	18.78	52674	42
<i>11</i>	14 26 08.71, +37 51 39.0	19.07	51671	54
<i>12</i>	14 26 11.55, +37 50 23.3	18.87	48309	138
<i>13</i>	14 26 11.10, +37 50 22.2	18.18	46889	42
<i>14</i>	14 26 09.48, +37 50 16.6	18.61	50578	64
<i>15</i>	14 26 05.55, +37 50 59.4	20.24	99106	156
<i>16</i>	14 26 07.62, +37 50 03.1	19.64	52026	76
<i>17</i>	14 26 04.48, +37 50 29.4	17.91	50718	38
<i>18</i>	14 26 06.25, +37 49 46.0	18.55	48881	36
<i>19</i>	14 26 04.38, +37 49 57.1	18.91	46491	94
<i>20†</i>	14 26 03.89, +37 49 53.4	16.39	50251	54
<i>21</i>	14 26 02.75, +37 49 53.9	18.51	50453	48
<i>22</i>	14 26 02.57, +37 49 51.3	17.44	50634	40
<i>23</i>	14 26 03.08, +37 49 24.7	18.58	49457	38
<i>24</i>	14 25 58.19, +37 50 20.2	18.72	50348	36
<i>25</i>	14 26 00.46, +37 49 19.7	18.28	49297	42
<i>26</i>	14 26 00.17, +37 49 10.2	18.14	51825	40
<i>27</i>	14 25 58.19, +37 49 18.5	17.90	48730	50
<i>28</i>	14 25 58.05, +37 49 01.4	—	50168	70
<i>29‡</i>	14 25 56.67, +37 48 59.2	15.87	51029	26
<i>30</i>	14 25 57.37, +37 48 19.4	19.75	51092	74
<i>31</i>	14 25 55.12, +37 48 38.4	19.08	48103	50
<i>32</i>	14 25 54.55, +37 48 33.0	19.14	49759	50
<i>33</i>	14 25 56.50, +37 47 40.9	19.64	63968	68
<i>34</i>	14 25 51.99, +37 48 32.3	18.35	49702	30
<i>35</i>	14 25 53.88, +37 47 29.5	17.23	48844	26
<i>36</i>	14 26 07.98, +37 49 10.3	19.09	50582	64
<i>37</i>	14 25 59.57, +37 49 40.0	17.37	50669	60
<i>38</i>	14 25 54.63, +37 50 42.5	18.62	49378	82
<i>39</i>	14 25 57.93, +37 49 29.4	18.18	50600	36

could affect this selection, we executed the shifting gapper method, but now considering the BCG2 as cluster center. This procedure selected identical galaxy members. That is, in our case, the galaxy member selection, and so the dynamical analysis here exposed is not affected by the choice of the cluster center. So, we decided to consider the BCG1 as cluster center, as in agreement with Okabe & Umetsu (2008).

3.2 Global cluster properties

By using the biweight method (Beers et al. 1990, ROS-TAT software) with the 89 cluster members, we obtained a mean cluster redshift of $\langle z \rangle = 0.1678 \pm 0.0004$, i.e. $\langle v \rangle = (50\,313 \pm 140) \text{ km s}^{-1}$. In addition, by applying the same method and correcting for cosmological effects and

³ see the URL <http://www2.cadc-ccda.hia-ihp.nrc-cnrc.gc.ca/megapipeline/docs/proc.html#photcal> for a comparison between Megacam and SDSS filters.

[!ht]

Table 1. Continued.

ID	α, δ (J2000)	r^{Mega}	v (km s ⁻¹)	Δv
40	14 25 57.04, +37 49 24.0	19.15	52796	88
41	14 25 56.71, +37 48 35.2	18.93	50818	66
42	14 25 58.94, +37 46 44.8	18.08	55204	76
43	14 25 54.86, +37 47 27.5	19.04	63647	134
44	14 25 47.88, +37 48 42.7	17.70	52746	34
45	14 25 45.91, +37 48 59.0	18.25	49070	44
46	14 25 53.16, +37 46 25.4	18.40	51371	30
47	14 25 49.61, +37 47 12.9	17.93	55809	54
48	14 25 39.45, +37 49 43.2	17.69	50257	32
49	14 25 42.80, +37 48 24.8	18.66	63410	82
50	14 25 41.21, +37 48 33.1	19.25	49330	66
51	14 25 50.13, +37 45 40.2	19.37	48884	42
52	14 25 43.62, +37 47 09.4	18.52	55791	78
53	14 25 41.30, +37 47 21.5	19.60	49661	154
54	14 25 43.18, +37 46 28.8	19.28	107888	102
55	14 25 37.68, +37 47 16.4	18.53	49832	70
56	14 25 38.15, +37 46 47.5	19.53	51154	76
57	14 25 35.19, +37 46 57.4	19.62	52210	140
58	14 25 37.35, +37 45 28.0	19.17	49115	50
59	14 26 00.79, +37 51 26.5	19.42	49776	142
60	14 25 59.08, +37 51 38.0	20.07	52324	198
61	14 26 03.33, +37 49 58.7	18.69	50782	86
62	14 26 01.96, +37 49 49.2	—	48245	98
63	14 26 01.79, +37 49 27.9	19.15	49258	74
64	14 25 55.03, +37 51 00.7	18.45	49768	34
65	14 25 52.49, +37 50 35.7	18.53	48045	98
66	14 25 58.32, +37 48 40.3	19.94	50783	122
67	14 25 55.51, +37 48 24.9	19.36	63942	116
68	14 25 55.10, +37 48 18.9	19.65	136183	142
69	14 25 52.18, +37 48 13.4	18.68	50039	70
70	14 25 49.51, +37 48 36.0	18.59	50373	92
71	14 25 53.42, +37 47 11.2	19.64	49720	110
72	14 25 46.80, +37 48 33.1	18.93	51359	96
73	14 25 47.80, +37 47 48.0	18.70	52710	226
74	14 25 47.16, +37 47 32.7	19.84	50831	102
75	14 25 45.39, +37 46 38.2	18.75	51263	72
76	14 25 32.10, +37 49 42.1	19.94	52009	122
77	14 25 35.57, +37 47 55.9	18.80	51456	156
78	14 25 33.46, +37 47 57.8	21.05	80056	101

standard velocity errors (Danese et al. 1980), we obtained $\sigma_V = 1210_{-110}^{+125}$ km s⁻¹ (errors were estimated using the bootstrap technique). However, in order to check the robustness of this estimate, we study the variation of σ_V with the distance to the cluster center (Fig. 4, bottom panel). The integral σ_V profile is flat, suggesting that the estimation of σ_V is robust. Furthermore, when considering members within $0.1 h_{70}^{-1}$ Mpc from the BCGs (that is two groups of 7 and 8 galaxy members around BCG1 and BCG2, respectively), we measure similar mean velocities. We only find a modest difference, being $\langle v \rangle_{\text{BCG2}} < \langle v \rangle_{\text{BCG1}}$, which is in agreement with the finding that $v_{\text{BCG2}} < v_{\text{BCG1}}$ (see also section 3.5).

3.3 The small high velocity group

Figure 4 (top panel) shows that most of the interlopers have a very similar high velocity. We assign eight galaxies to a

[!ht]

Table 1. Continued.

ID	α, δ (J2000)	r^{Mega}	v (km s ⁻¹)	Δv
79	14 25 30.98, +37 47 42.2	19.72	107174	52
80	14 25 34.12, +37 46 19.4	19.63	63240	146
81	14 25 33.41, +37 46 12.7	18.57	45921	120
82	14 25 40.35, +37 50 40.8	17.95	49856	26
83	14 25 41.46, +37 50 37.9	19.52	47584	100
84	14 25 30.96, +37 48 56.2	20.48	83757	122
85	14 25 42.09, +37 49 49.6	19.56	51428	78
86	14 25 44.52, +37 49 60.0	18.17	50404	60
87	14 25 41.35, +37 48 53.7	21.00	49505	268
88	14 25 50.54, +37 49 58.0	18.46	50589	76
89	14 25 36.49, +37 47 37.6	18.77	55764	140
90	14 25 57.98, +37 50 23.9	19.99	53193	126
91	14 25 49.31, +37 48 58.9	20.49	63713	212
92	14 25 56.55, +37 49 45.4	17.43	55190	76
93	14 26 00.35, +37 50 04.3	17.88	48048	74
94	14 25 47.90, +37 48 00.0	16.68	39699	60
95	14 25 47.86, +37 47 40.3	19.48	55602	110
96	14 25 48.93, +37 47 40.5	18.77	50226	244
97	14 25 53.51, +37 48 05.9	17.88	46140	150
98	14 25 56.78, +37 47 54.6	18.98	64149	234
99	14 25 42.34, +37 45 37.4	20.02	52653	100
100	14 25 56.75, +37 47 27.0	19.59	55676	100
101	14 25 54.29, +37 46 51.5	20.42	53514	126
102	14 25 52.73, +37 45 45.9	18.49	62209	44
103	14 25 49.27, +37 45 04.7	18.83	48960	80
104	14 25 52.09, +37 45 16.2	19.67	145911	156
105	14 26 09.38, +37 47 29.2	18.65	52566	46
106	14 25 49.55, +37 44 32.2	19.19	50106	46
107	14 26 01.01, +37 45 49.6	18.61	47775	100
108	14 26 07.52, +37 46 31.9	19.20	50245	80
109	14 25 51.38, +37 43 58.6	19.98	82764	132
110	14 25 51.90, +37 43 49.7	19.43	58839	152
111	14 25 57.45, +37 44 19.9	19.63	63715	164
112	14 25 50.55, +37 43 08.8	19.36	24748	100
113	14 25 59.89, +37 44 11.9	19.12	50613	60
114	14 25 59.47, +37 50 54.1	17.33	49944	52
115	14 26 06.58, +37 51 28.3	17.18	49226	59
116	14 25 29.47, +37 47 00.1	17.30	49505	37
117	14 26 19.25, +37 48 43.5	17.19	49969	51
118	14 25 49.81, +37 53 04.0	17.66	50095	43
119	14 26 22.97, +37 54 01.9	17.36	51262	44

likely galaxy group (red squares in Fig. 4, top panel). Seven out of these eight galaxies lie in the southwest cluster region, thus reinforcing the idea that this is a real structure. For this high velocity galaxy group (hereafter HVG) we estimate $\langle v \rangle_{\text{HVG}} = (55\,557 \pm 89)$ km s⁻¹ and $\sigma_{V,\text{HVG}} = 221_{-46}^{+55}$ km s⁻¹.

3.4 Velocity distribution and 3D substructure

Deviations from Gaussianity in the velocity distribution are interpreted as an important sign that clusters present a complex dynamics (Ribeiro et al. 2011).

In order to check the Gaussianity in the velocity distribution, we used three profile estimators. These are the skewness, the kurtosis, and the scaled tail index STI (see Bird &

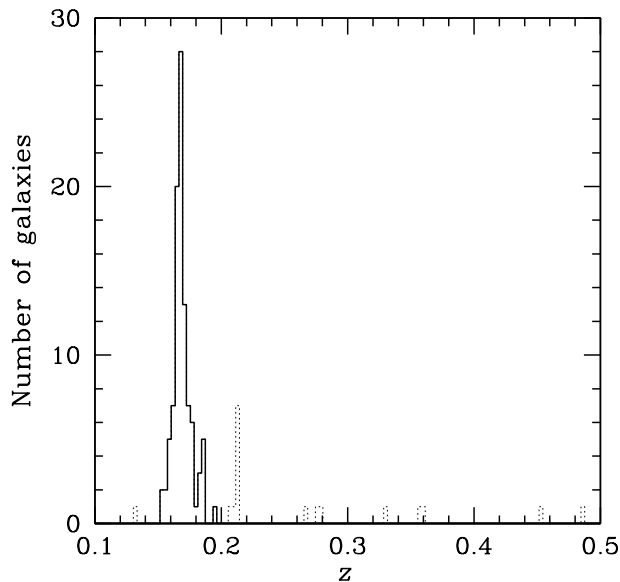


Figure 3. Redshift galaxy distribution. Solid line shows the histogram corresponding to the 100 (provisional) galaxies assigned to A1914 by the 1D-DEDICA reconstruction method.

Beers 1993). The STI finds evidence for non-Gaussianity at about 95%-99% c.l., suggesting a heavy tailed distribution (see Bird & Beers 1993 and their Table 2).

Furthermore, we investigated the presence of gaps in the velocity distribution. By using the weighted gap analysis presented by Beers et al. (1991; 1992; ROSTAT software), we detect one significant gap at the 97% c.l.. This gap divides A1914 into two groups, composed of 9 and 80 galaxies at low and high velocities, respectively. By applying the 2D Kolmogorov-Smirnov test (Fasano & Franceschini 1987) we see that the galaxies of the two groups present the same spatial distribution (see Fig. 5).

We also applied the 1D-Kaye’s mixture model (Ashman et al. 1994; see also, e.g., Boschini et al. 2012) – hereafter 1D-KMM – to search for bimodal partitions significantly fitting to the velocity distribution. The most likely solution (well under the 90% significance c.l.) indicates two groups of 15 and 74 galaxies, spatially not differing. Considering the KMM results, which take into account the group membership probability, we obtain that the two groups differ for about $\sim 140 \text{ km s}^{-1}$ in the cluster rest-frame ($\langle v \rangle_{\text{KMM1D-LV}} = 50155$ and $\langle v \rangle_{\text{KMM1D-HV}} = 50319 \text{ km s}^{-1}$) and the high velocity group has a much higher velocity dispersion ($\sigma_{\text{V,KMM1D-HV}} \sim 980 \text{ km s}^{-1}$ vs. $\sigma_{\text{V,KMM2D-LV}} \sim 330 \text{ km s}^{-1}$).

Correlations between spatial and velocity distributions of cluster galaxies usually indicate the presence of actual substructures. With this idea in mind, we used several techniques to reveal the structure of A1914 by combining positions and velocities. First, we searched for velocity gradients in the plane of the sky by performing multiple linear fits. The results of this test reveals no evidences of gradients. In addition, we performed a set of 3D tests: the classical Δ statistics (Dressler & Schechtman 1988), as well as its variation which considers separately mean velocity and velocity

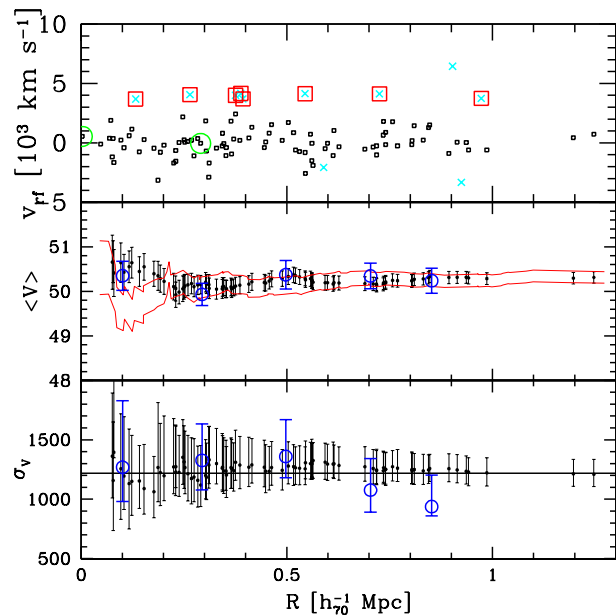


Figure 4. *Top panel:* rest-frame velocity vs. projected distance (BCG1 is assumed as the cluster center) for the all 100 galaxies within the velocity peak. Large green circles correspond to the location of the two brightest cluster galaxies. Cyan crosses show galaxies rejected as interlopers with the “shifting gapper” method. Galaxies belonging the HVG group are indicated with red squares. *Middle panel:* differential (blue circles) and integral (black dots) profiles of mean velocity for the 89 cluster members. We compute differential values within five annuli, each of $\sim 0.2 h_{70}^{-1} \text{ Mpc}$, from the cluster center. The integral profiles consider mean velocities of all galaxies within a given distance. The first value is obtained from the five inner galaxy members. Error bars show uncertainties at 68% c.l.. The band within red lines indicates the integral mean velocity when using BCG2 as the cluster center. *Bottom panel:* The same as middle panel but for the σ_v profiles. The horizontal line represents the value for the X-ray temperature (9 keV) transformed into σ_v assuming a $\beta_{\text{spec}} = 1$ model for the density-energy distribution between ICM and galaxies (see Sect. 4).

dispersion kinematical indicators (Girardi et al. 1997; Ferrari et al. 2003); the α -test (West & Bothun 1990) and the ϵ -test (Bird 1994) based on the projected mass predictions. None of the above mentioned tests yielded positive detection of substructures. Moreover, we found no substructure by applying the technique developed by Serna & Gerbal (1996), also named the “Htree-method” (see also, Durret et al. 2010; Boschini et al. 2012).

3.5 2D galaxy distribution of the spectroscopic catalog

We applied the 2D adaptive-kernel technique (hereafter 2D-DEDICA) to the spatial distribution of member galaxies. This method found only one significant peak, lying close to BCG2 and elongated toward BCG1. Figure 7 shows that A1914 presents an elongated profile in the NE-SW direction, suggesting a bimodal structure. To further investigate this point we applied the 2D-KMM method using as seeds the cluster members contained within $0.1 h_{70}^{-1} \text{ Mpc}$ from BCG1

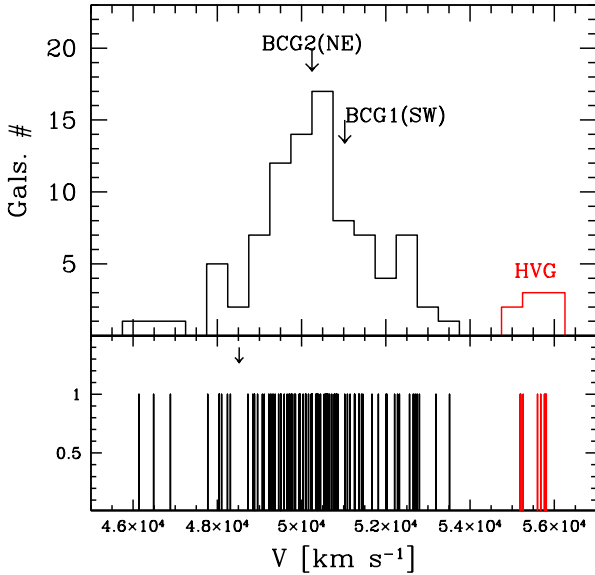


Figure 5. *Upper panel:* Velocity distribution of the galaxy members (black line) and to the HVG (red line). Velocities of BCG1 and BCG2 are also indicated by arrows. *Lower panel:* Streak density diagram of cluster members (black) and HVG members (red). The significant gap in the velocity distribution is indicated by an arrow.

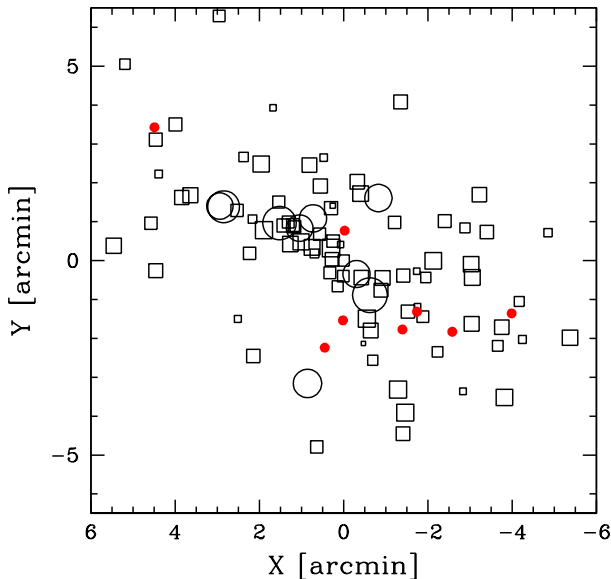


Figure 6. Projected spatial distribution of 89 cluster members (open symbols) and the 8 members of HVG (red solid circles). The size of symbols is directly correlated with the value of the radial velocity for each galaxy. Circles and squares indicate the two groups at low and high velocities, as detected through the weighted gap analysis. The plot is centered on the BCG1 position.

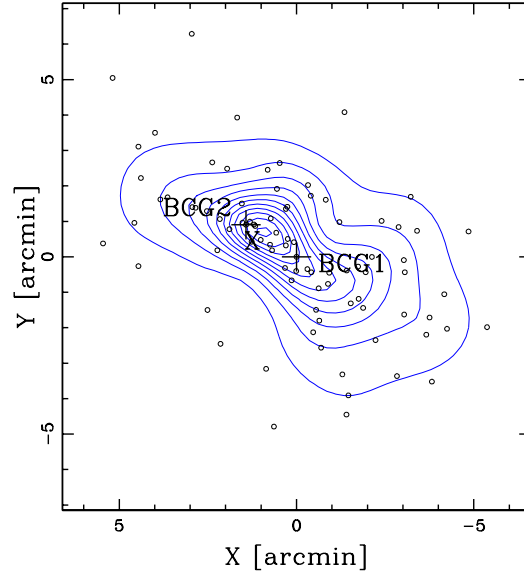


Figure 7. Projected spatial distribution with relative isodensity contours of spectroscopic cluster members (small circles). The density map has been obtained with the 2D-DEDICA method. BCG1 position is assumed as the cluster center. Both BCG1 and BCG2 locations are shown by crosses. The "X" indicates the X-ray peak (Govoni et al. 2004).

and BCG2 (7 and 8 galaxies, respectively). The method detects a bimodal solution, significant at the 99.6% c.l., with the KMM2D-SW group of 65 galaxies at south-west and the KMM2D-NE group of 24 galaxies at north-east (but note that both BCG1 and BCG2 are now both assigned to the SW group). When applying the 3D-KMM method we still found a bimodal solution with two groups of 69 (SW) and 20 galaxies (NE), with BCG1 and BCG2 assigned to the SW and NE groups, respectively. However, the significance of the 3D result is only at the 96% c.l., thus indicating that velocities do not give a positive contribution to the separation of the two substructures. In fact, according to the Kolmogorov-Smirnov test, there is no difference between the velocity distributions of the two 3D groups.

3.6 2D galaxy distribution of the photometric catalogs

Our spectroscopic sample does not map the whole cluster field, besides of suffering for magnitude incompleteness. To overcome these restrictions we resorted to the photometric catalogs.

Using the CFHT photometry, we construct ($g'-r'$ vs. r') color-magnitude relation (hereafter CMR, see Fig. 8), and select likely early-type members within the red sequence (RS) locus. In order to compute the RS, we apply a 2σ -clipping fitting procedure to the spectroscopic cluster galaxies. We obtained $g^{\text{Mega}}-r^{\text{Mega}} = 1.341 - 0.021 \times r^{\text{Mega}}$ on 63 spectroscopic cluster members. With this method we selected as likely cluster members the objects within ± 0.2 mag with respect to the RS. Figure 8 shows as the selected magnitude intervals seem adequate to select RS galaxies. In this way, we only use good tracers of the cluster galaxy popula-

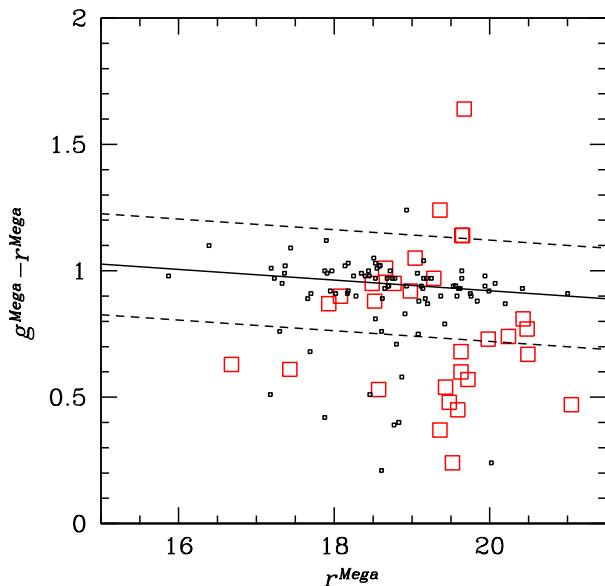


Figure 8. CFHT $g^{\text{Mega}} - r^{\text{Mega}}$ vs. r^{Mega} diagram for galaxies with available spectroscopy. Black and red squares indicate member and non-member galaxies. The solid line gives the CMR determined on member galaxies; the dashed lines are drawn at ± 0.2 mag from this value.

tion (e.g., Lubin et al. 2000). However, Fig. 8 suggests that our selection of photometric members is somewhat contaminated by several non members, probably because A1914 is contained in a rich large scale structure (see in the following).

Figure 9 shows the isodensity contours of likely cluster galaxies in three different magnitude bins considering the CFHT photometry. The three bins contain a comparable number of galaxies (from 2065 to 2377 in the whole CFHT area). A1914 is well detected using the most luminous galaxies and, as expected due to contamination problems, the noise increases at fainter magnitudes. The results for $r^{\text{Mega}} > 22$ are likely very contaminated by background systems (see below) and are shown for comparison. Through the photometric sample we can assess that the cluster structure is really NE-SW elongated and that the highest peak is not centered on BCG1. The precise position of the highest peak depends on the magnitude bin or on the catalog, however it is close to BCG2. In addition, using CFHT data we found an important secondary peak lying at south west of BCG1. In the $r' < 21$ sample, the two peaks are separated by $\sim 2.5'$, i.e. $\sim 0.4 h_{70}^{-1}$ Mpc at the cluster distance.

We also note that the external regions of A1914 are particularly rich of structures. Figure 9 shows the position of four galaxy clusters listed by NED: 1. NSCS J142452+373753 at $z \sim 0.17$ (identified in the Digitized Second Palomar Observatory Sky Survey DPOSS, Lopes et al. 2004; and then in SDSS); 2. 400d J1425+3758 at $z \sim 0.17$ (identified in the 400 Square Degree ROSAT PSPC Galaxy Cluster Survey, Burenin et al. 2007); 3. NSCS J142638+375327 at $z \sim 0.20$; 4. GMBG J216.49530+37.62102 at $z \sim 0.23$ (identified in the SDSS DR7, Hao et al. 2010). When using the best sample (the one

Table 2. 2D substructure detected in the CFHT photometric data.

2D – Subclump ($r = r^{\text{Mega}}$)	N_S	α, δ (J2000) 14 : m : s, +37 : ' : ''	ρ_S	χ^2_S
NE ($r < 21$)	167	26 : 02.2, 49 : 46	1.00	104
SW ($r < 21$)	176	25 : 52.0, 48 : 12	0.54	53
No.2 ($r < 21$)	204	25 : 02.2, 57 : 57	0.27	44
No.1 ($r < 21$)	99	24 : 49.4, 37 : 56	0.20	26
NE ($21 \leq r < 22$)	90	26 : 06.7, 49 : 53	1.00	24
SW ($21 \leq r < 22$)	96	25 : 53.0, 48 : 52	0.86	18
No.3 ($21 \leq r < 22$)	46	26 : 30.8, 54 : 25	0.62	15
No.2 ($21 \leq r < 22$)	80	25 : 30.4, 59 : 13	0.62	13

with $r^{\text{Mega}} < 21$), the two clusters closest in redshift (N.1 and N.2) are well detected, while the clusters N.3 and N.4 are better detected in the deeper magnitude ranges, thus confirming us that we are including more and more interlopers among our likely cluster members when considering fainter galaxies.

Table 2 lists information for the four highest, significant peaks in the galaxy distribution using the CFHT data: the estimated number of likely members, N_S (Col. 2); Equatorial coordinates of the substructure (Col. 3); the relative isodensity respect the highest peak, ρ_S (Col. 4); the χ^2 for each clump (Col. 5). Galaxy clusters No.1 and No.4 are detected as significant peaks in the $21 \leq r^{\text{Mega}} < 22$ sample, too, but having lower density.

4 DISCUSSION

We estimate a high value of the velocity dispersion, $\sigma_V = 1210^{+125}_{-110}$ km s $^{-1}$. This result well agrees with a hot ICM showing a mean $T_X \sim 9$ keV (Baldi et al. 2007 and Maughan et al. 2008) when assuming energy equipartition between galaxies and gas energy per unit mass⁴, i.e. $\beta_{\text{spec}} = 1$, both suggesting a massive galaxy cluster. In the following sections we discuss our findings on the dynamical mass and cluster structure. Thus, based on these results, we propose a two-body model and time scale for the collision of substructures in Abell 1914.

4.1 Mass estimates

We computed the global virial quantities assuming the dynamical equilibrium (but see in the following) and in the framework of usual assumptions, i.e. cluster sphericity and coincidence in the galaxy-mass distributions. Following the method detailed in Girardi & Mezzetti (2001, see also Girardi et al. 1998) we obtained R_{vir} , an estimation of R_{200} , and the mass within this radius. We assume a quasi-virialized region of $R_{\text{vir}} = 0.17 \times \sigma_V / H(z) h_{70}^{-1}$ Mpc (see Eq. 1 of Girardi & Mezzetti 2001 with the corresponding scaling of $H(z)$ from Eq. 8 of Carlberg et al.

⁴ $\beta_{\text{spec}} = \sigma_V^2 / (kT_X / \mu m_p)$ with $\mu = 0.58$ the mean molecular weight and m_p the proton mass.

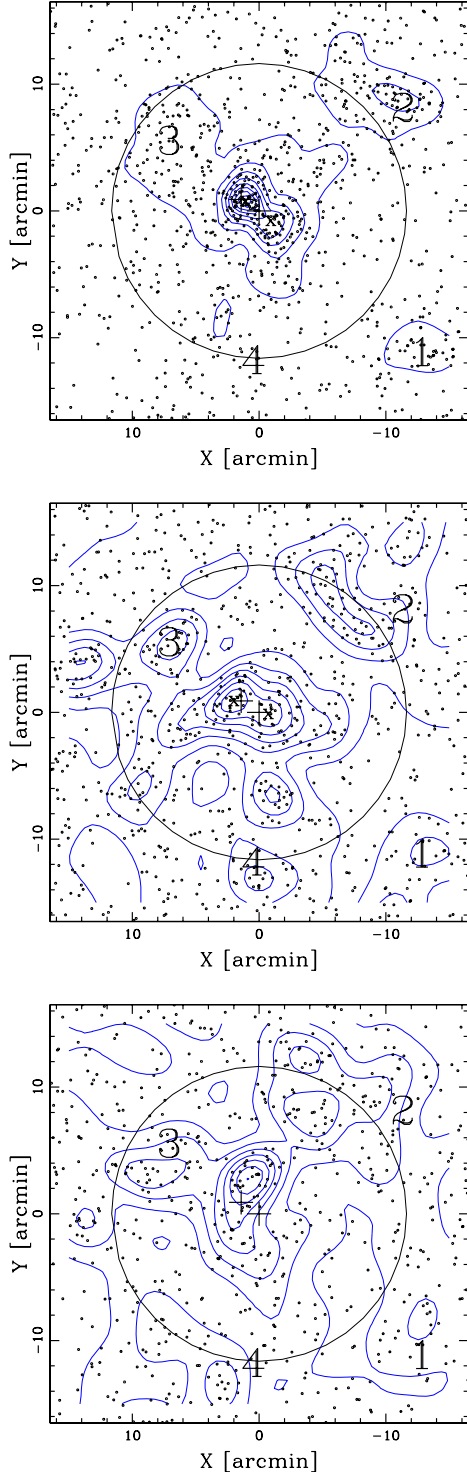


Figure 9. Projected spatial distribution and isodensity contours (CFHT likely galaxy members with $r^{\text{Mega}} < 21$ (*Top panel*), $21 \leq r^{\text{Mega}} < 22$ (*Middle panel*), and $22 \leq r^{\text{Mega}} < 22.5$ (*Bottom panel*). Contours were estimated using the 2D-DEDICA method. "x" symbols note the NE and SW clumps in the upper and middle panel, while "+" symbols mark the position of BCG1 and BCG2. The numbers indicate the positions of the four galaxy clusters listed by NED within $20'$ from the cluster center and having estimated or photometric redshift close to A1914 ($\Delta z < 0.06$), in order of increasing Δz . The circles indicate the cluster region within $2 h_{70}^{-1}$ Mpc at the cluster distance, i.e. somewhat smaller than the virial radius ($2.2\text{--}2.7 h_{70}^{-1}$ Mpc, which is determined by the adopted model).

1997 for R_{200}). We estimate the mass using the equation $M = M_{\text{vir}} - SPT = 3\pi/2 \cdot \sigma_V^2 R_{\text{PV}}/G - SPT$ (Eq. 3 of Girardi & Mezzetti 2001, with R_{PV} derived as described in Eq. 13 of Girardi et al. (1998), with $A = R_{\text{vir}}$ as a close approach, and being the surface pressure term correction (SPT) a 20% of M_{vir} . Both R_{vir} and M were estimated considering the velocity dispersion with the usual scaling-laws, where $R_{\text{vir}} \propto \sigma_V$ and $M(< R_{\text{vir}}) \propto \sigma_V^3$. We obtained $M(< R_{\text{vir}} = 2.7 h_{70}^{-1} \text{Mpc}) = 2.6 \pm 0.8 \times 10^{15} h_{70}^{-1} M_{\odot}$.

On the other hand, it is commonly accepted that A1914 hosts a merging event, and so velocity dispersion and X-ray temperature could be enhanced (e.g., Ricker & Sarazin 2001; Schindler & Müller 1993). Our analysis fails to separate the cluster substructures in the velocity space. We have to assume the result derived from the 1D-KMM method (Sect. 3.4, i.e. the two best Gaussians obtained there, despite their low significance. According to these results, the secondary group presents a very small velocity dispersion and its mass can be neglected with respect to the main system. For the main system $\sigma_{V,\text{main}} \sim 980 \text{ km s}^{-1}$ which leads to $M(< R_{\text{vir}} = 2.2 h_{70}^{-1} \text{Mpc}) = 1.4 \times 10^{15} h_{70}^{-1} M_{\odot}$. Hereafter, we consider as reliable the mass range $M_{\text{sys}} = 1.4\text{--}2.6 \times 10^{15} h_{70}^{-1} M_{\odot}$ for the whole A1914 system.

The above value of $\sigma_{V,\text{main}}$ is in agreement with $\sigma_{V,\text{SIS}} = 846 \pm 87$ estimated from the weak lensing analysis by Okabe & Umetsu (2008). For a punctual comparison with the projected mass computed by Okabe & Umetsu (2008) within $R=7'$, we project and rescale our mass estimate M_{sys} assuming the cluster follows a NFW profile, taking a mass concentration parameter c from Navarro et al. (1997) and correcting by the factor $1+z$ (Bullock et al. 2001; Dolag et al. 2004, here $c \sim 4$). We obtain $M_{\text{sys},2D}(< R = 1.2 h_{70}^{-1} \text{Mpc}) = (1.1\text{--}2.0) \times 10^{15} h_{70}^{-1} M_{\odot}$, in agreement with that $M_{2D}(< R = 7') = (4.10 \pm 1.55) \times 10^{14} h_{70}^{-1} M_{\odot}$ is a lower bound to the true enclosed mass (Okabe & Umetsu 2008). Instead, there is some tension between our value of $\sigma_{V,\text{main}}$ and the velocity dispersion estimate computed using redshifts from the on-going Hectospec Cluster Survey (Rines et al. 2010), $\sigma_{V,\text{Rines}} = 698_{-38}^{+46} \text{ km s}^{-1}$. This explains the difference between our and their virial mass estimate $M_{200,\text{Rines}} \sim 6.0 \times 10^{14} h_{70}^{-1} M_{\odot}$, as obtained rescaling the value of M_{100} ($R_{100} \sim 1.3 R_{200}$ and thus $M_{200} \sim 0.9 M_{100}$ for a NFW profile (Eke et al. 1996).

4.2 Cluster structure

Our 2D analyses confirm the existence of an important bimodal structure elongated in the NE-SW direction and find two significant peaks: the NE one closer to BCG2 and the SW one closer to BCG1, although not perfectly centered on the two BCGs.

The analysis of Govoni et al. (2004) shows that the X-ray peak is displaced with respect to the BCGs positions. They find that X-ray maximum is at South with respect to BCG2 (see their Fig. 5a). Similarly, we also find that the X-ray peak does not coincide with our peaks in the galaxy density (see our Fig. 1). The offset between the optical and X-ray peaks suggests a post-merger cluster but, as noted by Govoni et al. (2004), the X-ray features are not typical (e.g., simulations by Roettiger et al. 1998). In fact, their analysis shows the presence of a NE-SW arclike hot region crossing through the cluster center, while the X-ray emission is elon-

gated in the WNW-ESE direction, somewhat perpendicular to that described by the two galaxy/mass concentrations. Govoni et al. (2004) interpreted this observational scenario as due to a large impact parameter merger.

We add four contributes to the comprehension of the A1914 merging scenario. These contributes are: 1) the relative importance of the NE and SW subclusters; 2) the merger is likely most contained in the plane of the sky, as suggested by the failure of 1D and 3D substructure analysis methods in detecting the two galaxy subclumps (Pinkney et al. 1996); 3) A1914 is embedded in a rich large scale structure that suggests that cluster accretion happens along two specific directions, NE-SW and NW-SE; 4) the presence of HGV, a minor external group of uncertain nature.

Point 1. The NE subcluster, close to BCG2 and the X-ray peak, has higher density than the SW subcluster, close to BCG1. However, the SW subcluster is the richer - and likely the more massive as shown by the respective galaxy population at end of Sect. 3.5 and Table 2, and by the respective velocity dispersions). This agrees with the result of the gravitational lensing analysis by Okabe & Umetsu (2008), where the peak C1, which is related to BCG2, is the highest density peak in the mass distribution, while the second density peak, C2 related to BCG1, is suggested to be the primary cluster center.

The point 2. suggests a similarity between A1914 and the well-known cluster Abell 754 (hereafter A754). A754 is a bimodal cluster where two obvious substructures collide in the plane of the sky, showing an X-ray emission profile elongated and perpendicular to that of the two optical clumps (Zabludoff & Zaritsky 1995). The X-ray peak is closer to the denser optical peak, reminding us once more the similarity with A1914. As for A754, the gross X-ray morphology has been firstly explained with a non-zero impact parameter (Henry & Briel 1995), but more recent and detailed analyses suggest a more complex merger scenario, possibly involving a third substructure or a mass of cool gas disengaged from its previous host galaxy group and presently sloshing (Markvitch et al. 2003). In fact, a shock is found in front of the denser optical peak, as usual in head-on mergers (Macario et al. 2011).

Point 3. According to their estimated redshift, both galaxy systems No.1 and 2 are likely to be connected to A1914. No.1, i.e. the cluster NSCS J142452+373753 (Lopes et al. 2004), lies at SW. This and the merger axis of the two subclusters strongly supports the idea that A1914 is accreting groups from a filament aligned with the NE-SW direction. No.2, i.e. the cluster 400d J1425+3758 (Burenin et al. 2007), is a massive system (with $T_X > 5$ keV since included in the 400 Square Degree ROSAT PSPC Galaxy Cluster Survey) lying at NW, at the border of the virial radius of A1914, somewhat along the direction of the NW-SE elongated bright feature of the radio emission. Thus, No.2 traces the NW-SE direction of a likely second filament accreting onto the cluster. This suggests a merging scenario more complex than the simple bimodal one for A1914.

Point 4. The group HVG, although very poor, is also clearly detected as a separate group in the projected phase space (see Fig. 4). Its nature is instead not clear. In this sense, we think that the main collision between the two substructures may have produced out-flying galaxies as predicted by simulations (e.g., Czoske et al. 2002; Sales et al.

2007) and detected in a few clusters (e.g., in Abell 3266 by Quintana et al. 1996 and Flores et al. 2000; in Cl0024+1654 by Czoske et al. 2002). This hypothesis is supported by the fact that the system has not a circular morphology but 6 out of 8 galaxies trace a large strip. Moreover, 4 out of 8 galaxies show emission lines, thus suggesting a possible star forming activity triggered by the cluster merger. Alternatively, HVG could be a group in pre-collision phase with A1914, as well as a completely unbound group. Anyway, it is likely so poorly massive that can be considered a secondary detail in the cluster dynamics.

4.3 Bimodal model

In this section, we present our efforts to unravel the dynamics of the merger between the two main subclusters in the SW-NE direction with a simple bimodal model, assuming that this collision causes (at least part of) the diffuse radio emission. Following the method detailed for other DARC clusters (see e.g., Abell 520 in Girardi et al. 2008 and Abell 2345 in Boschin et al. 2010), we apply the two-body model (Beers et al. 1982; Thompson 1982) to evaluate the timescales of the merger. This simple model assumes two point-mass bodies and a zero impact parameter. The model takes into account three parameters. These are the mass of the whole system, M_{sys} ($1.4\text{--}2.6 \times 10^{15} h_{70}^{-1} M_\odot$, see above), the relative line of sight velocity in the rest-frame, ΔV , and the projected linear distance between the two substructures, D . As for the relative motion parameters, we consider our more reliable results, i.e. the estimate $\Delta V = 140 \text{ km s}^{-1}$ obtained from our 1D analysis, and the estimate $D \sim 0.4 h_{70}^{-1} \text{ Mpc}$ obtained from our 2D analysis. Due to the small radiative life of relativistic electrons and as a comparison with other radio halos clusters (e.g., Barrera et al. 2002; Girardi et al. 2008), we assume an elapsed time, t , for the core crossing of few fractions of Gyr. We consider two different cases: $t = 0.1 \text{ Gyr}$ and $t = 0.3 \text{ Gyr}$.

Figure 10 compares the model solutions as a function of α , where α is the projection angle between the plane of the sky and the line connecting the centers of the two clumps, with the mass estimate of the system M_{sys} . At $t = 0.1 \text{ Gyr}$, the solution is bound and outgoing (BO) with $\alpha \sim 10^\circ - 25^\circ$, in agreement with the fact that we expect a merging axis mostly contained in the plane of the sky. At $t = 0.3 \text{ Gyr}$, the model predicts unlikely angles $\alpha > 60^\circ$. Even when considering as M_{sys} the virial mass value by Rines et al. (2010, see our Sect. 4.1), the model with $t \sim 0.1 \text{ Gyr}$ should be preferred.

5 CONCLUSIONS

In conclusion, A1914 shows clear evidence of a recent cluster merger along the NE-SW direction and almost contained in the plane of the sky. The presence of an ongoing merger and the large mass are the main features of typical clusters with radio halos described in the literature. The large scale structure in the environment of A1914 suggests evidence of a second direction of cluster accretion, NW-SE. This merging axis is likely related to the bright feature of the diffuse radio emission. Thus, we argue that the unusual radio appearance of A1914 is due to the complexity of the merger. Indeed,

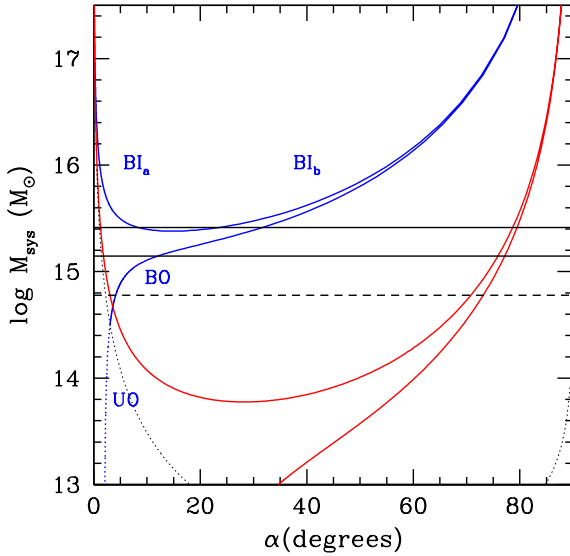


Figure 10. Two-body model applied to the NE and SW galaxy subclusters. The solutions are plotted as system mass vs. projection angle. Thick solid and thick dotted curves are bound and unbound solutions, respectively. Blue and red lines correspond to the case of $t = 0.1$ and $t = 0.3$ Gyr, respectively. BI_a and BI_b labels refer to bound and incoming, which denote the collapsing solutions (solid curve). On the other hand, the expanding solutions and unbound outgoing solutions (solid curve going on in the dotted curve, respectively) are labeled as BO and UO. Labels for the $t = 0.3$ case are skipped to keep the figure clear. Our mass estimate is enclosed by the horizontal solid lines, while the dashed line is the mass value obtained by Rines et al. (2010). The Newtonian criterion predicts a limit for bound solutions; this limit is shown as the thin dashed curve (above and below is the bound and unbound regimes, respectively).

we point out that A1914 appearance resembles that of A754 where a complex merger scenario or a sloshing core seem to be the possible explanations. Only deeper X-ray data and many redshift measurements in a more extended cluster region could allow us to better understand the dynamics of A1914.

ACKNOWLEDGMENTS

We are in debt with Federica Govoni for the VLA radio image she kindly provided us. M.G. acknowledges financial support from PRININAF2010. This work has been supported by the Programa Nacional de Astronomía y Astrofísica of the Spanish Ministry of Science and Innovation under grants AYA2010-21322-C03-02, AYA2007-67965-C03-01 and AYA2010-21887-C04-04.

This publication is based on observations made on the island of La Palma with the Italian Telescopio Nazionale Galileo (TNG), which is operated by the Fundación Galileo Galilei – INAF (Istituto Nazionale di Astrofisica) and is located in the Spanish Observatorio de the Roque de Los Muchachos of the Instituto de Astrofísica de Canarias.

This research has made use of the NASA/IPAC Extragalactic Database (NED), which is operated by the Jet

Propulsion Laboratory, California Institute of Technology, under contract with the National Aeronautics and Space Administration.

This research has made use of archival data obtained at the Canada-France-Hawaii Telescope (CFHT), which is operated by the National Research Council of Canada, the Institut National des Sciences de l’Univers of the Centre National de la Recherche Scientifique of France, and the University of Hawaii.

This research has made use of the galaxy catalog of the Sloan Digital Sky Survey (SDSS). Funding for the SDSS has been provided by the Alfred P. Sloan Foundation, the Participating Institutions, the National Aeronautics and Space Administration, the National Science Foundation, the U.S. Department of Energy, the Japanese Monbukagakusho, and the Max Planck Society. The SDSS Web site is <http://www.sdss.org/>.

The SDSS is managed by the Astrophysical Research Consortium for the Participating Institutions. The Participating Institutions are the American Museum of Natural History, Astrophysical Institute Potsdam, University of Basel, University of Cambridge, Case Western Reserve University, University of Chicago, Drexel University, Fermilab, the Institute for Advanced Study, the Japan Participation Group, Johns Hopkins University, the Joint Institute for Nuclear Astrophysics, the Kavli Institute for Particle Astrophysics and Cosmology, the Korean Scientist Group, the Chinese Academy of Sciences (LAMOST), Los Alamos National Laboratory, the Max-Planck-Institute for Astronomy (MPIA), the Max-Planck-Institute for Astrophysics (MPA), New Mexico State University, Ohio State University, University of Pittsburgh, University of Portsmouth, Princeton University, the United States Naval Observatory, and the University of Washington.

REFERENCES

- Abell, G. O., Corwin, H. G. Jr., & Olowin, R. P. 1989, *ApJS*, 70, 1
- Ashman, K. M., Bird, C. M., & Zepf, S. E. 1994, *AJ*, 108, 2348
- Bacchi, M., Feretti, L., Giovannini, G., & Govoni, F. 2003, *A&A*, 400, 465
- Baldi, A., Ettori, S., Mazzotta, P., Tozzi, P., & Borgani, S. 2007, *ApJ*, 666, 835
- Bardelli, S., Zucca, E., Vettolani, G., et al. 1994, *MNRAS*, 267, 665
- Barrena, R., Biviano, A., Ramella, M., Falco, E. E., & Seitz, S. *A&A*, 386, 816
- Barrena, R., Girardi, M., Boschin, W., & Dasí, M. 2009, *A&A*, 503, 357
- Barrena, R., Girardi, M., Boschin, W., & Mardirossian, F. 2012, *A&A*, 540, A90
- Basu, K. 2012, *MNRAS*, 421, L112
- Beers, T. C., Flynn, K., & Gebhardt, K. 1990, *AJ*, 100, 32
- Beers, T. C., Forman, W., Huchra, J. P., Jones, C., & Gebhardt, K. 1991, *AJ*, 102, 1581
- Beers, T. C., Gebhardt, K., Huchra, J. P., et al. 1992, *ApJ*, 400, 410
- Beers, T. C., Geller, M. J., & Huchra, J. P. 1982, *ApJ*, 257, 23

- Bird, C. M. 1994, *AJ*, 107, 1637
- Bird, C. M., & Beers, T. C. 1993, *AJ*, 105, 1596
- Boschin, W., Barrena, R., & Girardi, M. 2010, *A&A*, 521, A78
- Boschin, W., Girardi, M., Barrena, R., & Nonino, M. 2012, *A&A*, 540, A43
- Brunetti, G., Cassano, R., Dolag, K., & Setti, G. 2009, *A&A*, 507, 661
- Brunetti, G., Setti, G., Feretti, L., & Giovannini, G. 2001, *MNRAS*, 320, 365
- Brunetti, G., Venturi, T., Dallacasa, D., et al. 2007, *ApJ*, 670, L5
- Bullock, J. S., Kolatt, T. S., Sigad, Y., et al. 2001, *MNRAS*, 321, 559
- Buote, D. A. 2002, in “Merging Processes in Galaxy Clusters”, eds. L. Feretti, I. M. Gioia, & G. Giovannini (The Netherlands, Kluwer Ac. Pub.): Optical Analysis of Cluster Mergers
- Buote, D. A., & Tsai, J. C. 1996, *ApJ*, 458, 27
- Burenin, R. A., Vikhlinin, A., Hornstrup, A., et al. 2007 *ApJS*, 172, 561
- Carlberg, R. G., Yee, H. K. C., & Ellingson, E. 1997, *ApJ*, 478, 462
- Cassano, R., Brunetti, G., & Setti, G. 2006, *MNRAS*, 369, 1577
- Cassano, R., Ettori, S., Giacintucci, S., et al. 2010, *ApJL*, 721, 82
- Czoske, O., Moore, B., Kneib, J.-P., & Soucail, G. 2002, *A&A*, 386, 31
- Dahle, H., Kaiser, N., Irgens, R. J., Lilje, P. B., & Maddox, S. J. 2002, *ApJS*, 139, 313
- Danese, L., De Zotti, C., & di Tullio, G. 1980, *A&A*, 82, 322
- Dolag, K., Bartelmann, M., Perrotta, F., et al. 2004, *A&A*, 416, 853
- Dressler, A., & Sackett, S. A. 1988, *AJ*, 95, 985
- Durret, F., Laganá, T. F., & Bertin, E. 2010, *A&A*, 517, A94
- Ebeling, H., Voges, W., Böhringer, H., et al. 1996, *MNRAS*, 281, 799
- Eke, V. R., Cole, S., Frenk, C. S., & Navarro, J. F. 1996, *MNRAS*, 281, 703
- Ellingson, E., & Yee, H. K. C. 1994, *ApJS*, 92, 33
- Ensslin, T. A., Biermann, P. L., Klein, U., & Kohle, S. 1998, *A&A*, 332, 395
- Ensslin, T. A., & Gopal-Krishna 2001, *A&A*, 366, 26
- Fadda, D., Girardi, M., Giuricin, G., Mardirossian, F., & Mezzetti, M. 1996, *ApJ*, 473, 670
- Fasano, G., & Franceschini, A. 1987, *MNRAS*, 225, 155
- Feretti, L., Giovannini, G., Govoni, F., & Murgia, M. 2012, *A&A*, 20, 54
- Ferrari, C., Govoni, F., Schindler, S., Bykov, A. M., & Rephaeli, Y. 2008, *Space Sci. Rev.*, 134, 93
- Ferrari, C., Maurogordato, S., Cappi, A., & Benoist C. 2003, *A&A*, 399, 813
- Flores, R. A., Quintana, H., & Way, M. J. 2000, *ApJ*, 532, 206
- Giovannini, G., & Feretti, L. 2002, in “Merging Processes in Galaxy Clusters”, eds. L. Feretti, I. M. Gioia, & G. Giovannini (The Netherlands, Kluwer Ac. Pub.): Diffuse Radio Sources and Cluster Mergers
- Giovannini, G., Feretti, L., Girardi, M., et al. 2011, *A&A*, 530, L5
- Giovannini, G., Tordi, M., & Feretti, L. 1999, *New Astronomy*, 4, 141
- Girardi, M., Bardelli, S., Barrena, R., et al. 2011, *A&A*, 536, A89
- Girardi, M., Barrena, R., & Boschin, W. 2010, Contribution to the conference “Galaxy clusters: observations, physics and cosmology”, held in Garching (Germany), July 26-30 2010. Published online at the site <http://www.mpa-garching.mpg.de/~clust10/>
- Girardi, M., Barrena, R., Boschin, W., & Ellingson, E. 2008, *A&A*, 491, 379
- Girardi, M., & Biviano, A. 2002, in “Merging Processes in Galaxy Clusters”, eds. L. Feretti, I. M. Gioia, & G. Giovannini (The Netherlands, Kluwer Ac. Pub.): Optical Analysis of Cluster Mergers
- Girardi, M., Escalera, E., Fadda, D., et al. 1997, *ApJ*, 482, 11
- Girardi, M., Fadda, D., Giuricin, G. et al. 1996, *ApJ*, 457, 61
- Girardi, M., Giuricin, G., Mardirossian, F., Mezzetti, M., & Boschin, W. 1998, *ApJ*, 505, 74
- Girardi, M., & Mezzetti, M. 2001, *ApJ*, 548, 79
- Govoni, F., Ensslin, T. A., Feretti, L., & Giovannini, G. 2001, *A&A*, 369, 441
- Govoni, F., Markevitch, M. L., Vikhlinin, A., et al. 2004, *ApJ*, 605, 695
- Gwyn, S. D. J. 2009, *PASP*, Conference Proceedings, 411, 123
- Hao, J., McKay, T. A., Koester, B. P. 2010, *ApJS*, 191, 254
- Henry, J. P., & Briel, U. G. 1995, *ApJ*, 443, L9
- Hoefl, M., Brüggén, M., & Yepes, G. 2004, *MNRAS*, 347, 389
- Kempner, J. C., & Sarazin, C. L. 2001, *ApJ*, 548, 639
- Keshet, U. 2010, preprint arXiv:1011.0729
- Komissarov, S. S., & Gubanov, A. G. 1994, *A&A*, 285, 27
- Jones, M. E., Edge, A. C., Grainge, K., et al. 2005, *MNRAS*, 357, 518
- Lopes, P. A. A., de Carvalho, R. R., Gal, R. R., et al. 2004, *AJ*, 128, 1017
- Lubin, L. M., Brunner, R., Metzger, M. R., Postman, M., Oke, J. B. 2000, *ApJL*, 531, 5
- Macario, G., Markevitch, M., Giacintucci, S., et al. 2011, *ApJ*, 728, 82
- Malumuth, E. M., Kriss, G. A., Dixon, W. Van Dyke, Ferguson, H. C., & Ritchie, C. 1992, *AJ*, 104, 495
- Markevitch, M., Gonzalez, A. H., David, L., et al. 2002, *ApJ*, 567, L27
- Markevitch, M., Mazzotta, P., Vikhlinin, A., et al. 2003, *ApJ*, 586, L19
- Maughan, B. J., Jones, C., Forman, W., & Van Speybroeck, L. 2008, *ApJS*, 174, 117
- Maurogordato, S., Sauvageot, J. L., Bourdin, H., et al. 2011, *A&A*, 525, A79
- Navarro, J. F., Frenk, C. S., & White, S. D. M. 1997, *ApJ*, 490, 493
- Okabe, N., & Umetsu, K. 2008, *PASJ*, 60, 345
- Pinkney, J., Roettiger, K., Burns, J. O., & Bird, C.M. 1996, *ApJS*, 104, 1
- Pisani, A. 1993, *MNRAS*, 265, 706
- Pisani, A. 1996, *MNRAS*, 278, 697
- Quintana, H., Carrasco, E. R., & Reisenegger, A. 2000, *AJ*, 120, 1017

- 120, 511
- Quintana, H., Ramirez, A., & Way, M. J. 1996, *AJ*, 112, 36
- Ribeiro, A. L. B., Lopes, P. A. A., & Trevisan, M. 2011, *MNRAS*, 413, 81
- Ricker, P. M., & Sarazin, C. L. 2001, *ApJ*, 561, 621
- Rines, K., Geller, M. J., & Diaferio, A. 2010, *ApJL*, 715, 180
- Roettiger, K., Burns, J. O., & Stone, J. M. 1999, *ApJ*, 518, 603
- Roettiger, K., Loken, C., & Burns, J. O. 1997, *ApJS*, 109, 307
- Roettiger, K., Stone, J. M., & Mushotzky, R. F. 1998, *ApJ*, 493, 62
- Rossetti, M., Eckert, D., Cavalleri, B. M., et al. 2011, *A&A*, 532, 123
- Sales, L. V., Navarro, J. F., Lambas, D. G., White, S. D. M., & Croton, D. J. 2007, *MNRAS*, 382, 1901
- Schindler, S. & Müller, E. 1993, *A&A*, 272, 137
- Schuecker, P., Böhringer, H., Reiprich, T. H., & Feretti, L. 2001, *A&A*, 378, 408
- Serna, A., & Gerbal, D. 1996, *A&A*, 309, 65
- Struble, M. F. & Rood, H. J. 1987, *ApJS*, 63, 555
- Thompson, L. A. 1982, in *IAU Symposium 104, Early Evolution of the Universe and the Present Structure*, eds. G. O. Abell and G. Chincarini (Dordrecht: Reidel)
- Tonry, J., & Davis, M. 1979, *ApJ*, 84, 1511
- Venturi, T. 2011, *Mem. Soc. Astron. Italiana*, 82, 499
- West, M. J., & Bothun, G. D. 1990, *ApJ*, 350, 36
- Zabludoff, A. I., & Zaritsky, D. 1995, *ApJ*, 447, L21